Eur. Phys. J. A (2016) **52**: 79
DOI 10.1140/epja/i2016-16079-0

THE EUROPEAN PHYSICAL JOURNAL A

Review

Techniques and methods for the low-energy neutrino detection*

Gioacchino Ranucci[a]

INFN, Sezione di Milano, Via Celoria 16 - 20133 Milano, Italy

Received: 7 July 2015
Published online: 8 April 2016 –
Communicated by C. Broggini

Abstract. Low-energy neutrino physics and astrophysics has been one of the most active field of particle physics research over the past two decades, achieving important and sometimes unexpected results, which have paved the way for a bright future of further exciting studies. The methods, the techniques and the technologies employed for the construction of the many experiments which acted as important players in this area of investigation have been crucial elements to reach the many accumulated physics successes. The topic covered in this review is, thus, the description of the main features of the set of methodologies at the basis of the design, construction and operation of low-energy neutrino detectors.

1 Introduction

The neutrino detection techniques encompass several different methodologies of widespread use in the general field of particle detection. The multiplicity of detection methods is enhanced by the plurality of experimental needs posed by the several neutrino sources of experimental interest, which are solar neutrinos, atmospheric neutrinos, reactor neutrinos, geoneutrinos (*i.e.* anti-neutrinos from Earth), neutrinos from accelerators, supernova neutrinos and neutrinos from astrophysical sources.

The many facets of experimental neutrino field find almost naturally their counterpart in the variety of techniques applied by the experimentalists to cover this broad range of application: radiochemical methods, water Cherenkov detector, heavy water detector, large water Cherenkov detector under sea or ice, scintillation techniques, time projection chambers, nuclear emulsions. However, not all these techniques will be covered in this review, which is instead focused on the subset of topics more specifically connected to the realm of low-energy neutrino detection. Therefore, the attention in the following is focused to the radiochemical methods, which found extensive applications in the pioneers studies on solar neutrinos, to the water Cherenkov detectors (included the heavy-water version), which provided epochal results in the assessment of the neutrino oscillations through the study of solar neutrinos and which marked the field with the historical first observation of neutrinos from a supernova, and to the scintillation detectors, which are the choice for most of the reactor experiments, as well as fundamental instruments for the challenging real time detection of sub-MeV low-energy solar neutrinos, and that provided as additional output the first detection of anti-neutrinos from Earth.

2 Radiochemical method

The radiochemical technique is the basis of the procedure exploited by the Homestake [1], Gallex/GNO [2] and Sage [3] experiments to detect solar neutrinos. The principle is very simple and elegant: the detection medium is a material which, upon absorption of a neutrino, is converted into a radioactive element whose decay is afterwards revealed and counted.

The pioneering Homestake experiment used a chlorine solution as a target for inverse β-interactions,

$$\nu_e + {}^{37}\mathrm{Cl} \rightarrow {}^{37}\mathrm{Ar} + e^-, \tag{1}$$

characterized by a threshold of 0.814 MeV. It is worth to remind that such a technique was proposed independently by two giants of modern physics, Bruno Pontecorvo and Louis Alvarez. Gallium experiments instead, adopted gallium as target, which allows neutrino interaction via

$$\nu_e + {}^{71}\mathrm{Ga} \rightarrow {}^{71}\mathrm{Ge} + e^-. \tag{2}$$

The threshold of this reaction is 233 keV, low enough to detect neutrinos from the initial proton fusion chain, which instead cannot be revealed with the chlorine reaction due to the higher threshold. Specific Standard Solar

* Contribution to the Topical Issue "Underground nuclear astrophysics and solar neutrinos: Impact on astrophysics, solar and neutrino physics" edited by Gianpaolo Bellini, Carlo Broggini, Alessandra Guglielmetti.

[a] e-mail: gioacchino.ranucci@mi.infn.it

Model estimates gives the following breakdown for the expected contributions to the gallium signal: pp-neutrinos 53%, ^{7}Be 27%, ^{8}B 12% and CNO 8%.

Two experiments have been implemented employing Gallium, Gallex/GNO at Gran Sasso and Sage at Baksan. In Gallex/GNO the target consisted of 101 tons of a $GaCl_3$ solution in water and HCl, containing 30.3 tons of natural gallium; this amount corresponds to about 10^{29} ^{71}Ga nuclei. The solution was contained in a large tank hosted in the Hall A of the underground Gran Sasso Laboratory.

^{71}Ge produced by neutrinos is radioactive and decay back by electron capture into ^{71}Ga. The mean life of a ^{71}Ge nucleus is about 16 days: thus the ^{71}Ge accumulates in the solution, reaching equilibrium when the number of ^{71}Ge atoms produced by neutrino interactions is just the same as the number of the decaying ones. When this equilibrium condition is reached, about a dozen ^{71}Ge atoms are present inside the whole gallium chloride solution. Therefore the solar neutrino flux above threshold is deduced from the number of ^{71}Ge produced atoms, using the theoretically calculated cross section. The challenging experimental task is thus to identify the feeble amount of ^{71}Ge atoms.

This is accomplished through a complex procedure which contemplates several steps:

a) The solution is exposed to solar neutrinos for about four weeks.
b) The ^{71}Ge atoms present at the end of the four week period in the solution are in the form of volatile $GeCl_4$, which is extracted into water by pumping about 3000 m^3 of nitrogen trough the solution.
c) The extracted ^{71}Ge is converted into gaseous GeH_4 and introduced into miniaturized proportional counters mixed with xenon as counting gas. At the end, a quantity variable between 95 and 98% of the ^{71}Ge present in the solution at the time of extraction is in the counter; extraction and conversion efficiencies are under constant control using non-radioactive germanium isotopes as carriers.
d) Decays and interactions in the counter are observed for a period of 6 months, allowing the complete decay of ^{71}Ge and a good determination of the counter background. The charge pulses produced in the counters by decays are recorded by means of fast transient digitizers.
e) The data, after application of suitable cuts, are then analyzed with a maximum likelihood algorithm to obtain the most probable number of ^{71}Ge introduced in the counter, with some final corrections applied to take into account possible extra-counts generated by high-energy muons from cosmic rays and by natural radioactivity.

Key issue in the overall procedure is the minimization of the possible sources of backgrounds, which is obtained by the rigorous application of low-level radioactivity technology in the design and construction of the counters, by the use in the analysis of pattern recognition techniques

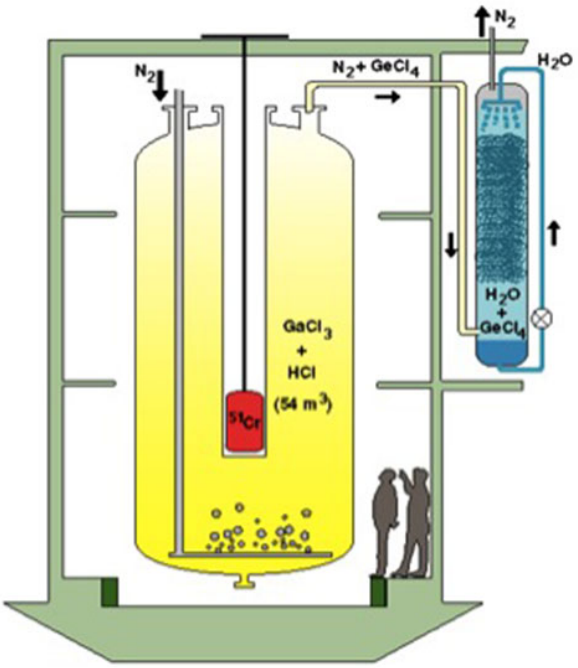

Fig. 1. Conceptual sketch of the Gallex set-up with the ^{51}Cr source in its centre.

able to discriminate signal and background events, and by the precise calibration of the counters via an external Gd/Ce X-ray source, to enhance the accuracy of the signal/background discrimination through the pattern recognition method.

Thanks to this sophisticated technique, the Gallium experiments were able to provide very important results in the studies of solar neutrinos, confirming unambiguously the discrepancy between the measured and predicted flux. To conclude, it is worth to mention another important ingredient of the radiochemical solar neutrino program, *i.e.* the source calibration efforts which were performed to prove unequivocally the validity of the entire neutrino detection concept implied by this technique. Details on this key experimental aspect can be found in Carla Cattadori, "Analyses methods in radiochemical experiments", paper published in this issue.

While the calibration procedure was globally very successful, a residual difference between the predicted and measured flux is one of the several anomalies in the in the neutrino sector, which taken together hint to a possible additional sterile state, a very hot topic in the current debate in the neutrino field.

For illustrative purposes, the Gallex set-up with the sketch of the source in its centre is depicted in fig. 1.

3 Cherenkov detector

The widespread diffusion of the Cherenkov technique in the field of neutrino physics is witnessed by the many experimental set-ups based on this methodology which have

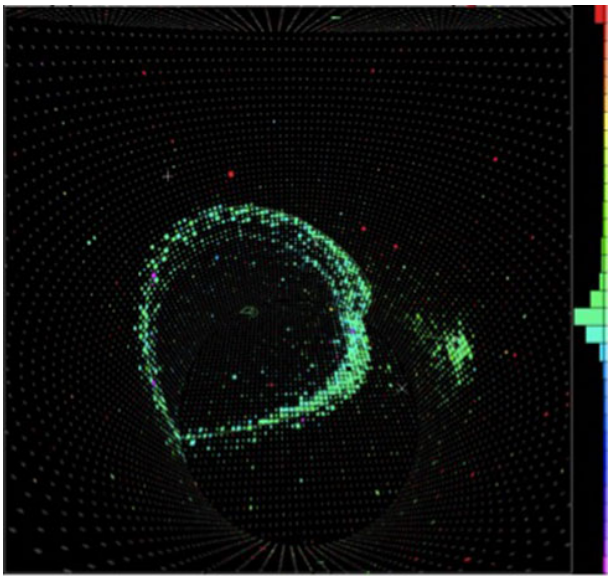

Fig. 2. A typical Cherenkov ring as seen in a large water detector like Super-Kamiokande.

been employed to investigate a large portion of the neutrino spectrum, from low to high energies.

The Cherenkov radiation is produced in a material with refractive index n by a charged particle if its velocity is greater than the local phase velocity of the light. The charged particle polarizes the atoms along its trajectory, generating time-dependent dipoles which in turn generate electromagnetic radiation. If $v < c/n$ the dipole distribution is symmetric around the particle position, and the sum of all dipoles vanishes. If $v > c/n$ the distribution is asymmetric and the total time-dependent dipole is different from zero, and thus radiates.

The resulting light wavefront is conical, characterized by an opening angle whose cosine is equal to $1/(\beta n)$; the spectrum of the radiation is ultra-violet-divergent, being proportional to $1/\lambda^2$. The propagation properties of the Cherenkov light are therefore fully equivalent to that of the acoustic Mach cone.

By observing the Cherenkov light in a large detector with an array of photomultipliers, the light cone is mapped into a very characteristic ring, like that shown as example in fig. 2 (from the Super-Kamiokande detector, see the next section, sect. 3.2). From the topological and timing features of the ring, the properties of the incoming particle can be inferred rather precisely.

3.1 SNO

A paradigmatic example of how the Cherenkov light can be used as basis to build a very effective neutrino detector is constituted by the SNO detector [4]. Located underground in Canada, in the Inco mine at Sudbury, this detector employed heavy water, which acted both as target medium for the neutrinos and as light generating material. The basic idea beyond the choice of heavy water is to perform two independent solar-neutrino measurements based on the deuterium target: the first is aimed to detect specifically the electron neutrino component, while the second is sensitive to the all flavour flux. Thus, the comparison of the two results can permit to unambiguously discern if neutrinos, generated only as electron neutrinos in the core of the Sun, undergo flavour conversion during the path Sun-Earth.

Heavy water makes this possible providing both flavour-specific and flavour-independent neutrino reactions. The first, flavour-specific reaction is the charged current reaction,

$$\nu_e + d \rightarrow p + p + e^-, \tag{3}$$

sensitive only to electron neutrinos.

As the neutrino approaches the deuterium nucleus, a W boson is exchanged, changing the neutron in deuterium to a proton, and the neutrino to an electron. Essentially all the neutrino energy is transferred to the electron. Due to the large energy of the incident neutrinos, the electron will be so energetic that it will be ejected at light speed, which is actually faster than the speed of light in water, therefore creating a burst of Cherenkov photons; after traveling throughout the water volume, they are revealed by the spherical array of photomultipliers instrumenting the detector. The amount of light is proportional to the incident neutrino energy, which can be inferred from the number of hits on the PMTs. From the hit pattern, also the angle of propagation of the light can be determined.

The second flavour-independent reaction is the so-called neutral current reaction

$$\nu_x + d \rightarrow p + n + \nu_x. \tag{4}$$

In this reaction a neutral Z boson is exchanged (hence the name of the reaction). The net effect is just to break apart the deuterium nucleus; the liberated neutron is then thermalized in the heavy water as it scatters around. The reaction can eventually be observed due to gamma rays which are emitted when the neutron is finally captured by another nucleus. The gamma rays will scatter electrons, which produce detectable light via the Cherenkov process, as discussed before.

The neutral current reaction is equally sensitive to all neutrino types; the detection efficiency depends on the neutron capture efficiency and the resulting gamma cascades. Neutrons can be captured directly on deuterium, but this is not very efficient. For this reason SNO has employed two separated neutral current systems to enhance the neutral current detection, the first based on the ^{35}Cl which has been added to the heavy water in form of NaCl, and the second constituted by proportional helium counters which have been deployed in the core of the detector.

There is also a third reaction occurring in the detector, flavour-independent as well, which is the electron scattering

$$\nu_x + e^- \rightarrow \nu_x + e^-. \tag{5}$$

This reaction is not unique to heavy water, being instead the primary mechanism in other light water detectors, like Kamiokande/Super-Kamiokande. Although this reaction

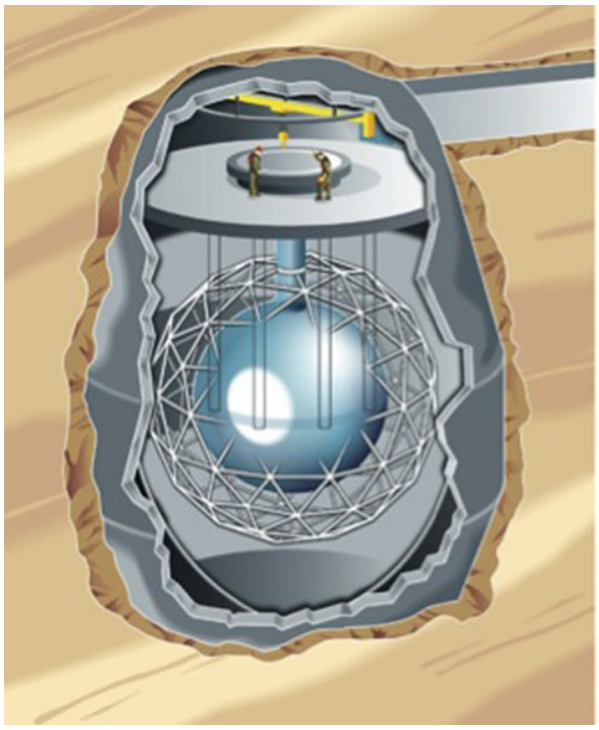

Fig. 3. Conceptual architectural scheme of the SNO detector.

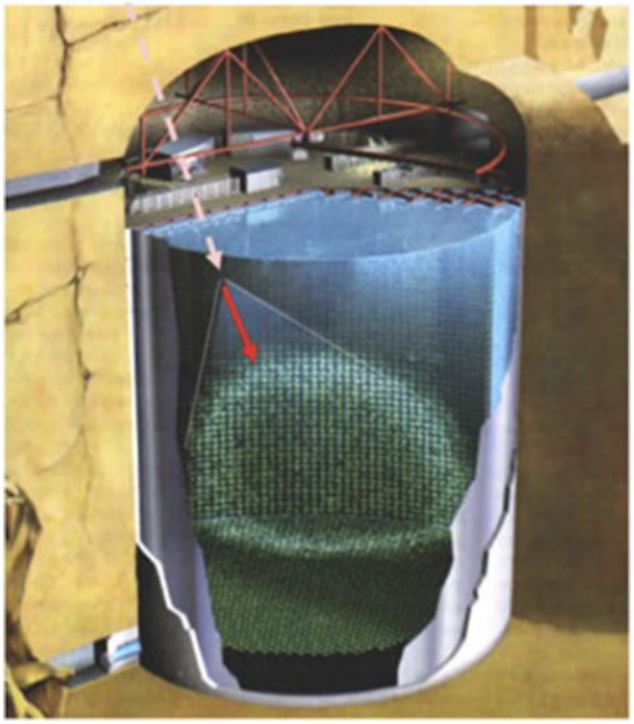

Fig. 4. Conceptual architectural scheme of the Super-Kamiokande detector.

is sensitive to all neutrino flavors, due to the different cross sections involved the electron neutrino dominates by a factor of six. The final-state energy is shared between the electron and the neutrino, thus there is very little spectral information from this reaction. On the other hand, good directional information can be obtained.

The general drawback affecting the Cherenkov technique is that, due to the feeble amount of light produced by the Cherenkov mechanism, the effective neutrino threshold is around 4–5 MeV, thus allowing the detection only of the high-energy component of the solar flux, essentially the ^{8}B neutrinos.

The SNO experiment is now completed, with the heavy water returned to the owner until the very last drop. Its architectural scheme was very simple (see fig. 3), aimed to get the most from the Cherenkov technique: 1000 tons of heavy water were contained in a thick transparent acrylic vessel, surrounded by an external layer of light water as shielding from the gammas from the radioactivity in the rock. A spherical array of 10000 phototubes detected the light from both volumes of water. A key issue for the success of the experiment was the long-standing effort throughout the construction and the operation phases to reduce the natural radioactivity in the target volume, not only uranium and thorium, but also in particular the ubiquitous radon gas. As a result, the multiple, clean and almost background-free, CC, NC and elastic scattering detection of solar neutrinos provided the unambiguous and model-independent proof that neutrinos from the Sun undergo flavour conversion, which was the key to unlock the mystery of the 30 years old solar neutrino problem. This achievement is the collective output of the three phases in which the experiment evolved, characterized by the different detection procedures of the neutrons signaling the occurrence of the neutral current reactions: a pure heavy water phase, a salt phase and the final ^{3}He counters stage [5].

3.2 Super-Kamiokande

As anticipated before, Super-Kamiokande [6], like its predecessor Kamiokande, is conceptually very similar to SNO, the major difference being the use of normal water instead of heavy water. Hence the neutrino detection occurs only via the scattering reaction off the electrons; the afterwards mechanism of Cherenkov light production and detection via an array of PMTs is equal to that already described for SNO.

Another major difference is the quantity of water employed, in total 50 ktons, which makes this detector the most massive among the solar neutrino experiments built so far, together with the geometry of the target, cylindrical instead spherical, as can be appreciated in fig. 4. The sufficiently high statistics implied by this huge volume has made possible a fairly precise reconstruction of the spectrum of the scattered electrons, which plays an important role in the subsequent analysis for the interpretation of the data.

The intrinsic high directionality of the scattering reaction, coupled to the directionality of the Cherenkov light, provides this experiment with a powerful tool to fight the background due to trace impurities of natural radioactivity dissolved in water, by associating the reconstructed

direction of the Cherenkov photons with the angular position of the Sun. Clearly, this is done on top of the purification procedure of the light water, which as for SNO was focused generally on the whole natural radioactivity, but with special emphasis on the radon, which is the factor limiting the threshold at low energy.

Contrary to SNO, Super-Kamiokande is still currently taking data. The long history of this detector started in 1996 and evolved through four phases: the first phase lasted until a major PMT incident in November 2001 and produced the most accurate measure up to now of the ^{8}B flux via the ES detection reaction. The phase II with reduced number of PMTs, from the end of 2002 to the end 2005, confirmed with larger error the phase-I measurement. After the refurbishment of the detector back to the original number of PMTs, the third phase lasted from the middle of 2006 up to the middle of 2008. After that, an upgrade of the electronics brought the detector into its fourth phase, which contemplates also an accelerator neutrino beam experiment, dubbed T2K. It is important to highlight the evolution of the energy threshold (total electron energy) in all the phases: 5 MeV in phase I, 7 MeV in phase II, 4.5 MeV in phase III and 3.5 MeV in phase IV, thanks to the continuously on-going effort to reduce the radon content in water.

4 Scintillation technique

The scintillation technique is very well suited to build massive experiments devoted to the detection of low-energy rare events. In particular in the neutrino field this method has been exploited fruitfully for reactor experiments (a very short list comprises Savannah river, Gosgen, Bugey, Chooz, Palo Verde, Kamland, Daya Bay, Reno, Double Chooz), accelerator experiments (LSND, Karmen, Nova) observatories for neutrinos from supernovae (LVD) and experiments for the detection of low-energy neutrinos from Sun (Borexino, that will be soon joined by SNO+).

Basically the scintillation method ensures the detection of ionising radiations through the light that it induces in special organic or inorganic materials [7,8]. Fundamental properties for a good scintillating material are the following: 1) high scintillation efficiency, 2) linear dependence (as much as possible) between energy deposit and emitted light, 3) limited self-absorption, 4) short decay time of the scintillation light, 5) suited to be shaped in several forms and dimensions, 6) refractive index similar to the glass, to ensure a good matching to the phototube.

As general introduction, it can be said that the light emission process comprises three mechanisms, denoted, respectively, as fluorescence, phosphorescence, and delayed fluorescence. Fluorescence is the main mechanism, represented by the prompt emission of visible radiation after the excitation of the material either by energetic particles or by incident light of suitable wavelength, while phosphorescence is the subsequent (parasitic) emission of visible radiation characterized by longer wavelength and longer decay time than fluorescence. A hybrid characterization is that featured by the third process of delayed fluorescence, since it is constituted by emitted light of the same wavelength of the primary fluorescence, but with emission time substantially longer.

There are several scintillating materials of common use divided in two broad categories: the first is that of organic components in the form of plastics and liquids, as well as some crystals, realized with aromatic polycyclic hydrocarbons, containing one or more benzene rings C_6H_6 (included in this category there are also some special organic crystals like anthracene). The second is the family of alkali halide crystals, which are instead inorganic materials. The members of the former group, characterized by a fast time response, but also by limited emitted light, are well suited for beta spectroscopy and fast neutron detection. The latter, on the other hand, feature better light yield and linearity, at the price of a longer time response; thanks to the high Z and density, they are particularly good for gamma spectroscopy.

In the organic materials the fluorescence process takes place in transitions between the energetic levels of the single molecule, independently of its physical state. In the polycyclic aromatic hydrocarbons the molecular levels involved in the process are the so-called electronic levels π which stem from the trigonal hybridisation (sp^2) of the four valence electrons of the carbon atoms at the vertex of the hexagonal planar molecule C_6H_6.

In this framework it is useful to remind that the electron configuration of the carbon atom in the ground state is $1s^2 2s^2 sp^2$, while the configuration of the same atom ready for the chemical binding is $1s^2 2s 2p^3$, with the orbitals of the four valence electrons undergoing a spatial modification know as hybridisation process. There are three possible configurations for the hybridisation: the first is the tetraedic or sp^3 hybridisation, in which the four resulting orbitals are fully equivalent, being directed according to the vertex of a tetrahedron, forming mutually an angle of $109^\circ\ 28'$. Diamond and methane are example of compounds with this hybridisation; usually materials belonging to this class are not luminescent.

The second type of hybridisation is called trigonal, denoted sp^2, including one unaltered p orbital (which in the framework of this hybridisation is denoted with the greek letter π) and three equivalent orbitals (denoted as σ orbitals) stemming from the mixing of the original orbitals, and which are coplanar and oriented at 120 degrees. This is the typical hybridisation of the planar and luminescent molecules of the aromatic polycyclic hydrocarbons. The π orbital is symmetric with respect to the molecular plane of the σ bounds.

Finally the last hybridisation, diagonal or sp, is constituted by two unaltered p orbitals and two equivalent orbitals at 180 degrees, originating linear molecules as acetylene.

The benzene molecule C_6H_6 is the prototypal example of a scintillating molecule featuring the trigonal hybridisation. In benzene the σ orbitals interact as shown in fig. 5, giving rise to localized binds C-C and C-H. The six atomic orbitals π interact originating molecular orbitals (still denoted with π) completely spatially delocalised,

Fig. 5. The benzene ring, basis for any polycyclic aromatic hydrocarbon solvent used in the formulation of liquid scintillators.

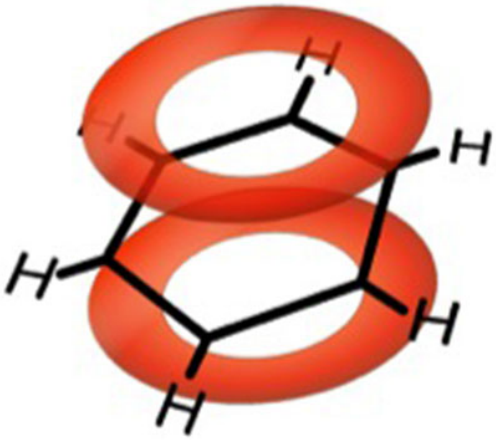

Fig. 6. Pictorial view of the delocalized π molecular orbitals in a benzene molecule.

whose excited states produce the molecular luminescence. The π delocalised orbitals are pictorially represented in fig. 6.

The energetic levels of the molecular orbitals π are schematically shown in fig. 7, where they are distinguished between spin 0 (singlet) levels, denoted as $S_0, S_1, S_2, \ldots$, and spin 1 (triplet) levels, denoted as $T_0, T_1, T_2, \ldots$. The dashed sublevels, whose spacing is about 0.15 eV, are vibrational molecular levels. The gap between the ground level S_0 and the first excited state S_1 is about 3 to 4 eV, depending upon the material. As shown in the figure, upon absorption of the incident radiation the molecule goes to an excited state, either the first excited states or beyond. In the latter case, the excited states higher than S_1 de-excite to S_1 through non-radiative internal conversion very rapidly, within few picoseconds (the vibrational sublevels S_{11}, S_{12} go promptly to S_{10}, too).

The fluorescence is constituted by the light emitted in the transition between the S_{10} level and one of the sublevels S_0. The characteristic fluorescence decay time

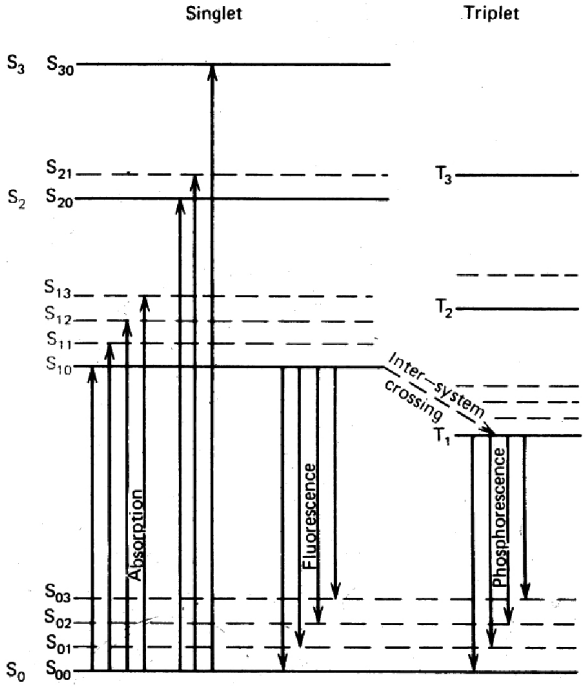

Fig. 7. Schematic representation of the energetic levels of the molecular orbitals π.

is thus the mean lifetime τ of the level S_{10}. To a good approximation, the decay profile of the light is a simple exponential function with τ as decay constant, which in the majority of the organic scintillators amounts to few nanoseconds.

On the other hand, the process of phosphorescence involves the triplet states; however, both creation of T_1 from S_0 and the inverse transition to S_0 from T_1 levels are highly inhibited because of the spin conservation condition. Actually, the molecules can be excited to the T_1 level via two indirect mechanisms, the non-radiative transition $S_1 \rightarrow T_1$ (called intersystem crossing) and the direct ionic recombination to T_1. The modest amount of phosphorescence light is originated in the (highly suppressed) transition T_1-S_1, which because of the relationship between the S_1 and T_1 levels (T_1 is below S_1, as shown in see fig. 7) is characterized by a longer wavelength. Since the transition is inhibited, the molecules can remain in the T_1 state for a long period, thus the time emission is characterized by decay times in the range of hundreds of microseconds.

The third luminescence mechanism, the delayed fluorescence, is due to the inverse transition T_1-S_1, followed by normal fluorescence decay. The inverse transition takes place according to the so-called triplet annihilation reaction $T_1 + T_1 \rightarrow S_1 + S_0 + \text{phonons}$. Hence its wavelength is that typical of the fluorescence process, while the decay time is dominated by the lifetime of the T_1 states, during which they can recombine to create the S_1 state, which immediately decays.

An important characteristic in the scintillation process is the wavelength distribution of the emitted light and conversely, the wavelength profile of the light inci-

dent on the scintillator which, in turn, can stimulate the emission. Both distributions, normally dubbed emission and absorption spectrum, depend upon the gaps between the levels (and sub-levels) S_1 and S_0. Since the scheme of fig. 7 shows that the excitation transitions require photons of energy higher than those resulting from the de-excitation process, the emission spectrum is shifted towards the right (longer wavelengths) with respect to the absorption one, with an overlapping region corresponding to the de-excitation S_{10}-S_{00}. In order to be useful for practical application a scintillator must be sufficiently transparent to its own light, which means that the overlapping region should span a limited wavelength range. The relative displacement of the two spectra is termed Stokes shift.

Another important feature of the scintillators is the scintillation efficiency, which is the fraction of the energy of the incoming radiation converted into visible light. In practice there are competing non-radiative de-excitation modes that limit the energy available for light production, one being clearly the heat production; all the others are generically called quenching, a term which groups several effects, some due also to possible impurities in the material. For example, in this respect the oxygen dissolved in liquid scintillators plays an important role since it is a powerful quenching factor, and thus has to be thoroughly removed from the scintillator.

Since hydrocarbon solvents feature the so-called energy migration process (*e.g.* the excitation, once created in a molecule can be easily transferred by that molecule to the surrounding molecules before the de-excitation occurs), the addition of a small quantity of a high efficiency solute gives a boost to the overall efficiency. The reason is that when the energy, throughout its migration from a molecule of the solvent to another, encounters a molecule of the additive at that point of the migration chain the conversion to light happens almost certainly. This is the rationality beyond the widespread use of binary components as plastic or liquid scintillators.

An important characteristic of great practical interest of several scintillator materials is the pulse shape discrimination. This feature is associated with the coexistence of the fluorescence and delayed fluorescence mechanisms. We said that that the fast fluorescence component is followed by a slow component originated by the two processes of delayed fluorescence and phosphorescence, whose origin is traced back to the presence of the triplet states T_1, featuring timing characteristics much longer than that of the fluorescence alone. Since the light fraction which is comprised in this long tail of the scintillation light depends upon the particle type, this characteristic of the scintillation process can be exploited to distinguish between different particles, hence the name of pulse shape discrimination associated to this scintillator property. In particular, since the density of the triplet states increases as function of the specific loss ($\mathrm{d}E/\mathrm{d}x$) of the incident particle, the tail of the light pulse is more pronounced for heavily ionising particles. A typical example of how this property is employed in practice is the discrimination between electron and alpha particles in applications where the background due to the natural radioactivity (mostly constituted by alpha radiations) must be eliminated from the measurement.

All the information generated in the scintillation mechanism is encoded in the associated light pulse. Usually, the data that the experimentalist need to extract from the light are the amplitude of the radiation, which is inferred from the amount of photons, and the time of the energy deposit. The latter can be unambiguously decoded if the overall pulse waveshape is very short. In typical organic scintillators ideally this is the case if the decay would be a simple exponential characterized by a unique time decay. While this is a good first-order approximation, this simplified picture is actually made more complex by the compositeness of the scintillation cocktails of practical use, so that for each additional component an additional exponential term is included in the description of the global decay profile; on top of this there is the further complication of the very long tail associated to the triplet states of the solvent. There are several experiments based on the liquid scintillator technique; a recent successful paradigmatic example is represented by the solar neutrino detector Borexino, described at length in the next paragraph.

4.1 Borexino

Borexino [9] is a scintillator detector which employs as active detection medium a mixture of pseudocumene (PC, 1,2,4-trimethylbenzene) and PPO (2,5-diphenyloxazole, a fluorescent dye) at a concentration of 1.5 g/l. Because of its intrinsic high luminosity (50 times more than in the Cherenkov technique) the liquid scintillation technology is extremely suitable for massive calorimetric low-energy spectroscopy. However, the lack of directionality of the method makes it impossible to distinguish neutrino scattered electrons from electrons due to natural radioactivity, as is done in the Cherenkov detector exploiting the association of the neutrino signals to the Sun direction. Therefore the crucial requirement of the Borexino technology is an extremely low radioactive contamination of the detection medium, at fantastic unprecedented levels, definitely below the acceptable limits in the water of SNO and Super-Kamiokande.

To reach ultra-low operating background conditions in the detector, the design of Borexino (see fig. 8) is based on the principle of graded shielding, with the inner scintillating core at the centre of a set of concentric shells of increasing radiopurity. The scintillator mass (278 ton) is contained in a 125 μm thick nylon Inner Vessel (IV) with a radius of 4.25 m. Within the IV a fiducial mass is software defined through the estimated events position, obtained from the PMTs timing data via a time-of-flight algorithm. A second nylon outer vessel (OV) with radius 5.50 m surrounds the IV, acting as a barrier against radon and other background contaminations originating from outside. The region between the inner and outer vessels contains a passive shield composed of pseudocumene and 5.0 g/l (later reduced to 3.0 g/l) of DMP (dimethylphthalate), a material that quenches the residual scintillation of PC so that

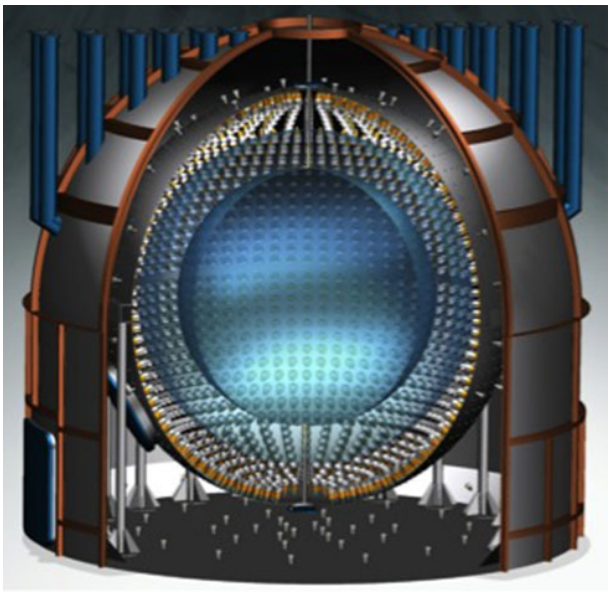

Fig. 8. Sketch of the Borexino experiment, highlighting its major components arranged according to a graded shielding design.

spectroscopic signals arise dominantly from the interior of the IV.

A 6.85 m radius stainless steel sphere (SSS) encloses the central part of the detector and serves also as a support structure for the PMTs. The region between the OV and the SSS is filled with the same inert buffer fluid (PC plus DMP) which is layered between the inner and outer vessels.

Finally, the entire detector is contained in a tank (radius 9 m, height 16.9 m) filled of ultra-pure water. The total liquid passive shielding of the central volume from external radiation (such as that originating from the rock) is thus 5.5 m of water equivalent (m.w.e). The scintillator material in the IV was less dense than the buffer fluid by about 0.1% with the original DMP concentration of 5 g/l; this resulted in a slight upward buoyancy force on the IV, implying the need of thin low-background ropes made of ultra-high-density polyethylene to hold the nylon vessels in place.

This modest buoyancy was further reduced of more than a factor 10 by removing via distillation a fraction of the total DMP content in the buffer: the process ended with a final DMP concentration of 3 g/l, still perfectly adequate to suppress the buffer scintillation, while at the same time appropriate to substantially prevent the outward scintillator flow from a small leaking point which developed on the vessel surface about 10 months after the start-up of the data taking.

The scintillation light is viewed by 2212 8″ PMTs (ETL 9351) uniformly distributed on the inner surface of the SSS. All but 371 photomultipliers are equipped with aluminium light concentrators designed to increase the collection efficiency of the light from the scintillator, and concurrently minimizing the detection of photons not coming from the active scintillating volume. Residual background scintillation and Cherenkov light that escape quenching in the buffer are thus reduced. The PMTs without concentrators can be used to study this background, as well as help identify muons that cross the buffer and not the inner vessel.

All the materials of the internal components of the detector (stainless steel, phototubes, cables, light concentrators, nylon) were specially selected for extremely low radioactivity. Furthermore, only qualified ultra-clean processes were employed for their realization, followed by careful surface cleaning methods.

The final assembly of the elements in the SSS was carried out in clean room conditions: the entire interior of the sphere was converted into a clean room of class 1000, while in front of the main entrance of the sphere itself an on-purpose clean room of class 100–1000 was used for all the final cleaning procedures of the equipment. Phototubes and ancillary mounting parts, light concentrators, calibration optical fibres, inner and outer vessels together with the anchoring systems, all passed and were treated through the access clean room, as well as the elaborated scaffolding system which was designed specifically to make it possible to the operators the safe and clean access to the whole sphere surface.

Clearly, for the success of the experiment key elements were also the many liquid purification and handling systems, which were designed and installed to ensure the proper manipulation of the fluids at the exceptional level demanded by Borexino. Without entering in the details of the complex layout and functionality of these plants, some salient points deserve to be mentioned.

The PC specially produced for Borexino, according to a stringent quality control plan developed jointly with the company, was shipped to the Gran Sasso location through special transport tanks cleaned, treated and prepared by us; the first operation there was the transfer of the PC via a dedicated unloading station to four big reservoir tanks, forming the so-called Storage Area, were the PC was stored prior to be inserted in the detector. Taken from the Storage Area, the PC was first purified via distillation, then either mixed with PPO for insertion in the Inner Vessel, or mixed with DMP for the insertion in the buffer region. Involved in this set of operations were the main Borexino plants: the Distillation Skids, the Filling Stations, the elaborate Interconnection system which allowed flexible transfers of the liquid throughout the various plants. Furthermore, the PPO was pre-mixed with a limited quantity of PC in a dedicated PPO System, originating a concentrated PPO solution which was then mixed in line with the PC at the level of the Filling Stations.

Other important ancillary plants, fundamental for the success of the operations, are the nitrogen systems, which delivered regular nitrogen, or on site purified nitrogen, or specially produced nitrogen with exceptionally low content of ^{39}Ar and ^{85}Kr, to be used for the crucial manipulations of the liquid in the inner vessel.

Finally, an ultra-pure-water system was used to produce the water for the cleaning operations, for the fill of the External Tank, and for the preliminary water fill of the Inner Detector.

Obviously, besides the design for the proper operating conditions, the cleanliness of the manufacturing processes used for the assembly of all these plants was of paramount importance for the success of Borexino, as well as the thorough and accurate cleaning procedures that they underwent upon their installation on site.

When data taking started in May 2007, it appeared immediately that the daunting task of the ultra-low radioactivity was successfully achieved, representing per se a major technological breakthrough, opening a new era in the field of ultra-pure detectors for rare events search.

The exceptional purity obtained implies that, once selected by software analysis the design fiducial volume of 100 tons and upon removal of the muon and muon-induced signals, the recorded experimental spectrum is so clean to show spectacularly the striking feature of the ^{7}Be scattering edge, *i.e.* the unambiguous signature of the occurrence of solar neutrino detection [10].

Other measurements provided by the experiment in its first years of operation are the ^{8}B spectrum with a threshold as low as 2.8 MeV [11], the absence of day-night asymmetry (as predicted by the MSW-LMA solution) in the ^{7}Be region [12], and the first measurement of the pep flux, made possible by the ultra-low background achieved by the experiment [13]; this last achievement required to cope with the background represented by the ^{11}C cosmogenic signals, exploiting the triple fold coincidence strategy devised on purpose by the Collaboration.

More recently, Borexino has achieved the milestone result of the first real time spectroscopic measurement of the fundamental pp flux [14]; such an historic measure has been made possible together by the low ^{14}C level of the scintillator, by the ultra-low background reached after the purification cycle, and by the very good energy resolution, which has opened and exploration window for the pp between 200 and 240 keV.

There are still additional solar results prospectively possible in the next years of running of the detector: per sure the improvements of the precision of all the solar fluxes measured so far, and, last but not least, the first measurement of the yet undetected CNO flux. The observation of the CNO would be undoubtedly the crowning of the solar program of Borexino, that, if this perspective will be confirmed, will conclude its operational life with the full solar spectroscopy of the entire solar neutrino flux, an epochal result accomplished by a single experiment.

4.2 Other experiments

Other important scintillator based experiments which provided milestone results for the understanding of the neutrino oscillation properties are KamLAND [15], and, more recently, Day Bay [16], Reno [17] and Double Chooz [18]. While in term of methodology all these experiments are very similar to Borexino, as far as detection criteria, techniques and architectural scheme are considered, their specific characteristics is the measurement target, constituted

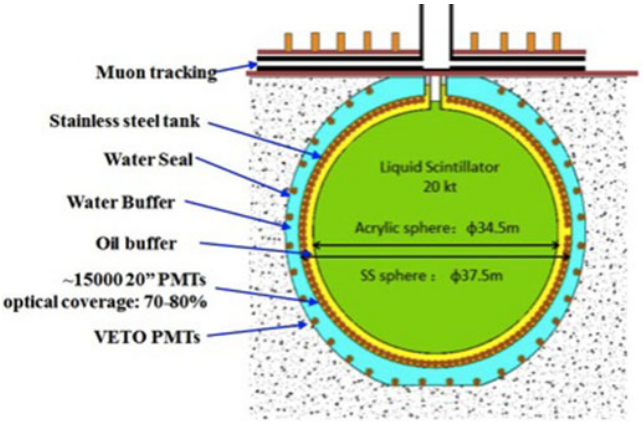

Fig. 9. Concept of the JUNO detector.

by anti-neutrinos from reactors. KamLAND, in particular, is not close to any specific reactor, but rather detects anti-neutrinos from a number of Japanese power plants located at an average distance of 200 km, thus performing a long-baseline test. Day Bay, Reno and Double Chooz, instead, are located a 1 km from the reactor, acting thus as medium baseline experiments.

While in general the respective technology resembles closely that of Borexino, there are some variations in the type of liquid scintillator, and in the material used for the balloon containing the liquid. The main difference with Borexino stems from the inverse beta reaction which is used to detect antineutrinos (in contrast with the scattering reaction adopted in Borexino to reveal neutrinos):

$$\overline{\nu_e} + p \rightarrow e^{+} + n. \tag{6}$$

After the occurrence of this interaction, the neutron thermalizes and is captured by a free proton, generating a typical 2.2 MeV gamma.

The mean time before the positron production and the neutron capture is about 256 μs, therefore the tight time coincidence between the respective light signals origins a correlated measurement which ensures a powerful discrimination of a true anti-neutrino detection with respect to the uncorrelated background events. This kind of signature greatly reduce the requirements for the suppression of the intrinsic radioactivity in the scintillator, marking the major difference between the technology of these reactor experiments and that employed for the solar neutrino detection in Borexino.

Historically, the measurement of KamLAND, together with that of SNO, closed the Solar Neutrino Problem, showing unambiguously that also reactor anti-neutrinos undergo the oscillation phenomenon, while concurrently determining rather precisely the associated mass squared difference parameter Δm_{21} and, jointly with the outputs of all other solar experiments, the mixing angle θ_{21}.

Day Bay, Reno and Double Chooz have the additional characteristics of being equipped with a near detector, so that the far-near arrangement allows determining also the θ_{13} mixing angle. An experiment that in a couple of years

will start data taking is SNO+ [19], the successor of the SNO detector. It is a liquid scintillator detector, as well, that can go on line soon thanks to the massive re-use of the SNO hardware and infrastructures. In particular the adoption of a new liquid scintillator, linear alkyl benzene, featuring the great advantage of being acrylic-compatible, will allow the re-use of the SNO acrylic vessel. Only the support system had to be built from scratch in order to cope with the different buoyancy condition with respect to the heavy water situation. The other major piece of equipment to realize is the purification system. The solar phase will be targeted mainly to pep and CNO detection, profiting of the depth of SNOLAB, which suppresses enormously the cosmogenic ^{11}C background. It should be, however, highlighted that the main goal of SNO+ will be the double beta decay with neodymium dissolved in the scintillator, and currently it is not yet decided whether the solar phase will come before or after the neodymium phase.

As final remark, we would like to underline that also the liquid scintillator technology is entering the stage of the gigantic detectors, which is more and more characterizing several fields of the modern particle physics, and that in our sector was initiated by the Cherenkov detectors. Plans for the 20 kton JUNO experiment [20] in China are well advanced; such a huge set-up, whose concept is schematically reported in fig. 9, will exploit the scintillation technology up to its farthest limit in order to unravel the last mysteries of the leptonic sector, in particular to determine the ordering of the neutrino masses.

5 Conclusions

The neutrino detection technology has reached a mature stage where different techniques coexist to cope with the multiple experimental challenges posed by the several investigated neutrino sources. In particular, Cherenkov, scintillator and radiochemical methods have proved to be essential in the long path towards the experimental assessment of neutrino oscillations.

Surely scintillator and Cherenkov methodologies will continue to play a fundamental role in the future research frontiers, from the highest (not covered here) to the lowest neutrino energy regions. In this interesting future, the achievement of ultra-low-background levels will continue to be a key experimental factor to ensure successful measurements, also in other rare process research field, like neutrinoless double-beta decay and dark matter searches.

References

1. B.T. Cleveland *et al.*, Astrophys. J. **496**, 505 (1998).
2. GALLEX Collaboration (W. Hampel *et al.*), Phys. Lett. B **447**, 127 (1999).
3. SAGE Collaboration (J.N. Abdurashitov *et al.*), Phys. Rev. C **80**, 015807 (2009).
4. J. Boger *et al.*, Nucl. Instrum. Methods A **449**, 172 (2000).
5. SNO Collaboration (B. Aharmim *et al.*), arXiv:1109.0763.
6. J. Hosaka *et al.*, Phys. Rev. D **73**, 112001 (2006).
7. J.B. Birks, *The theory and Practice of Scintillation Counting* (Pergamon Press, 1964) chapts. 3 and 6.
8. G.F. Knoll, *Radiation Detection and Measurement*, 3rd edition (Wiley, New York, 1999).
9. Borexino Collaboration (G. Alimonti *et al.*), Nucl. Instrum. Methods A **600**, 568 (2009).
10. Borexino Collaboration (G. Bellini *et al.*), Phys. Rev. Lett. **107**, 141302 (2011).
11. Borexino Collaboration (G. Bellini *et al.*), Phys. Rev. D **82**, 033006B8 (2010).
12. Borexino Collaboration (G. Bellini *et al.*), Phys. Lett. B **707**, 22 (2012).
13. Borexino Collaboration (G. Bellini *et al.*), Phys. Rev. Lett. **108**, 051302 (2012).
14. Borexino Collaboration (G. Bellini *et al.*), Nature **512**, 383 (2014).
15. KamLAND Collaboration (S. Abe *et al.*), Phys. Rev. Lett. **100**, 221803 (2008).
16. Daya Bay Collaboration (F.P. An *et al.*), Phys. Rev. Lett. **108**, 171803 (2012).
17. RENO Collaboration (J.K. Ahn *et al.*), Phys. Rev. Lett. **108**, 191802 (2012).
18. DOUBLE CHOOZ Collaboration (S. Abe *et al.*), Phys. Lett. B **723**, 66 (2013).
19. M. Chen, Nucl. Phys. B Proc. Suppl. **154**, 65 (2005).
20. Yu-Feng Li, Jun Cao, Yifang Wang, Liang Zhan, Phys. Rev. D **88**, 013008 (2013).